Asynchronous MASSLF Spectroscopy: A Convenient Method for Assigning Solid-State Carbon-13 CPMAS Spectra

Gretchen G. Webb† and Kurt W. Zilm*

Contribution from the Department of Chemistry, Yale University, 225 Prospect Street, New Haven, Connecticut 06511. *Received November 14, 1987*

Abstract: A two-dimensional solid-state NMR technique is presented which permits assignment of ^{13}C CPMAS spectra on the basis of the number of protons bonded to a carbon center. The method is similar to several other methods that have become popular for accurately determining C–H or N–H bond distances in solids and for following molecular motions in polymers. These techniques, referred to collectively as MASSLF spectroscopy, rely on the use of MAS NMR to resolve dipolar coupled patterns that would normally overlap in static one-dimensional spectra. The dipolar coupled patterns generated by these techniques are sufficiently sensitive that small variations in C–H distances in organic solids can be accurately measured. The patterns are, however, much more sensitive to the number of protons directly bonded to the carbon center. Under conditions of fast magic angle spinning, methylenes typically exhibit twice the number of sidebands as methines, and rapidly rotating methyl groups and nonprotonated carbons usually exhibit only one set of sidebands. The method presented here determines the number of methylenes, methines, and methyl plus nonprotonated carbons contributing to a resonance by taking advantage of the fact that the dipolar patterns have characteristic and predictable relative sideband intensities. A new MASSLF pulse sequence is used in this work that differs from previous sequences by not requiring synchronization with the MAS rotation. In addition the sequence conveniently allows for a much wider bandwidth in the dipolar dimension and produces the effect of quadrature detection in this frequency domain without the need for multiple data sets.

The combination of cross polarization[1] with magic angle spinning, CPMAS, has proven especially useful for obtaining high-resolution ^{13}C spectra of organic solids.[2-4] In the decade since its introduction, this method has found numerous applications in diverse fields such as polymers,[4] fossil fuels,[5] organic conductors,[6] carbocations,[7] and biochemistry.[8] Interpretation of CPMAS ^{13}C spectra has largely relied on comparison to the available data base of chemical shifts from solution ^{13}C NMR studies. The usual collection of methods for unambiguously assigning ^{13}C chemical shifts in solution are most often not applicable to solids. Typically this is the result of the complications brought on by the strong ^1H–^1H and ^1H–^{13}C dipolar couplings present in rigid solids.[9] This is an unfortunate situation as one of the principal attractions of solid-state NMR methods is that they can often be applied to systems in which solution NMR is not feasible and for which no solution analogues are available.[10,11]

To date there have been relatively few methods for assigning ^{13}C CPMAS spectra. The most commonly used technique is interrupted decoupling, alternatively known as dipolar dephasing.[12,13] This method is useful for discriminating between immobile protonated carbons and nonprotonated or very mobile protonated carbon centers. Some attempts have been made to make this technique quantitative; however, the state of the theory behind these methods is semiempirical at best.[14] Moreover, the method cannot effectively discriminate between methylene and methine carbons. A better separation between protonated and nonprotonated resonances in ^{13}C CPMAS spectra can be obtained with a one-dimensional magic angle spinning separated local field (MASSLF) method.[15] This technique has the advantage that it cleanly handles the linear phase correction errors present in interrupted decoupling even in the presence of very large chemical shift anisotropies (CSA). The theory needed to quantify the results in this case is cleaner and much more completely understood than for interrupted decoupling. However, this method still requires subtraction of two different spectra and also does not easily separate methylenes from methines. Other methods for spectral assignment of CPMAS spectra are adaptations of solution NMR methods for the solid state. Under certain conditions it has been shown that ^{13}C spectra with scaled ^1H–^{13}C J-couplings can be obtained with the appropriate proton-decoupling sequence. These methods have also been used for two-dimensional (2D) J spectroscopy in organic solids.[16] Unfortunately, these techniques are usually only applicable to systems in which molecular motion or magnetic dilution has already substantially reduced the ^1H–^1H dipolar couplings, thereby easing the requirements on the quality of the multiple pulse homonuclear decoupling.[17] A successful adaptation of heteronuclear shift correlation spectroscopy to solids has been reported by Roberts and co-workers.[18] This method has been successfully applied to rigid complex systems such as

†Present address: Department of Chemistry, Harvey Mudd College, Claremont, CA 91711.

(1) Pines, A.; Gibby, M. G.; Waugh, J. S. *J. Chem. Phys.* **1973**, *59*, 569-590.
(2) Schaefer, J.; Stejskal, E. O. *J. Am. Chem. Soc.* **1976**, *98*, 1031-1032.
(3) Stejskal, E. O.; Schaefer, J.; Waugh, J. S. *J. Magn. Reson.* **1977**, *28*, 105-112.
(4) Schaefer, J.; Stejskal, E. O.; Buchadahl, R. *Macromolecules* **1977**, *10*, 384-405.
(5) (a) Zilm, K. W.; Pugmire, R. J.; Larter, S. R.; Allan, J.; Grant, D. M. *Fuel* **1981**, *60*, 717-722. (b) Sullivan, M. J.; Maciel, G. E. *Anal. Chem.* **1982**, *54*, 1606-1615. (c) *Magnetic Resonance Introduction, Advanced Topics and Applications to Fossil Energy*; Petrakis, L., Fraissard, J. P., Eds. (NATO ASI Series); D. Reidel: Holland. (d) VanderHart, D. L.; Retcofsky, J. L. *Fuel* **1976**, *55*, 202.
(6) (a) Yannoni, C. S.; Clarke, T. C. *Phys. Rev. Lett.* **1983**, *51*, 1191-1193. (b) Toscano, P. J.; Marks, T. J. *J. Am. Chem. Soc.* **1986**, *108*, 437-444.
(7) (a) Yannoni, C. S.; Macho, V.; Myhre, P. C. *J. Am. Chem. Soc.* **1982**, *104*, 907-909. (b) Yannoni, C. S.; Macho, V.; Myhre, P. C. *J. Am. Chem. Soc.* **1982**, *104*, 7380-7381. (c) Lyerla, J. R.; Tannoni, C. S.; Bruck, D.; Fyfe, C. A. *J. Am. Chem. Soc.* **1979**, *101*, 4770-4772.
(8) Harbison, G. S.; Smith, S. O.; Pardoen, J. A.; Mulder, P. P. J.; Lugtenburg, J.; Herzfeld, J.; Mathies, R.; Griffin, R. G. *Biochemistry* **1984**, *23*, 2662-2667.
(9) VanderHart, D. L.; Earl, W. L.; Garroway, A. N. *J. Magn. Reson.* **1981**, *44*, 361-401.
(10) Zilm, K. W.; Merrill, R. A.; Greenberg, M. M.; Berson, J. A. *J. Am. Chem. Soc.* **1987**, *109*, 1567-1569.
(11) Dalling, D. K.; Zilm, K. W.; Grant, D. M.; Heeschen, W. A.; Horton, W. J.; Pugmire, R. J. *J. Am. Chem. Soc.* **1981**, *103*, 4817-4824.
(12) Opella, S. J.; Frey, M. H. *J. Am. Chem. Soc.* **1979**, *101*, 5854-5856.
(13) Munowitz, M. G.; Griffin, R. G.; Bodenhausen, G.; Huang, T. H. *J. Am. Chem. Soc.* **1981**, *103*, 2529-2533.
(14) Alemany, L. B.; Grant, D. M.; Alger, T. D.; Pugmire, R. J. *J. Am. Chem. Soc.* **1983**, *105*, 6697-6704.
(15) Raleigh, D. P.; Olejniczak, S. V.; Vega, S.; Griffin, R. G. *J. Am. Chem. Soc.* **1984**, *106*, 8302-8303.
(16) (a) Zilm, K. W.; Grant, D. M. *J. Magn. Reson.* **1982**, *48*, 524-526. (b) Terao, E.; Miura, H.; Saika, A. *J. Am. Chem. Soc.* **1982**, *104*, 5228-5229. (c) Miura, H.; Terao, T.; Saika, A. *J. Magn. Reson.* **1986**, *68*, 593-596. (d) Miura, H.; Terao, T.; Saika, A. *J. Chem. Phys.* **1986**, *85*, 2458-2462.
(17) Haeberlen, U. High Resolution NMR in Solids: Selective Averaging; *Advances in Magnetic Resonance, Suppl. 1*; Academic Press: New York, 1976.
(18) Roberts, J. E.; Vega, S.; Griffin, R. G. *J. Am. Chem. Soc.* **1984**, *106*, 524-526.

0002-7863/89/1511-2455$01.50/0

whole coals[19] and polymers[18] and is in general much more applicable than methods which rely upon resolvable scalar couplings. While promising, this 2D method critically depends on the quality of the proton homonuclear decoupling and, furthermore, only protonated carbons are observed.

Another way to assign ^{13}C chemical shifts is to determine the number of protons bonded directly to the carbon in question, i.e., its multiplicity. In solution ^{13}C NMR this is made possible by observation of scalar coupling patterns using one- or two-dimensional NMR techniques. This paper demonstrates that in the solid state this information is naturally obtained by 2D MASSLF methods which correlate ^{13}C chemical shifts with carbon–proton dipolar couplings.[13,20-22] Methods of this type were initially developed to determine ^{13}C–^{1}H and ^{15}N–^{1}H bond distances in organic solids.[13,23-25] These experiments have also been used to ascertain the orientation of chemical shift tensors in the molecular frame[13,26,27] and to study molecular motion in molecules and polymers.[28-31] Similar information is also obtained in 2D experiments that combine off-axis spinning during the SLF t_1 evolution with spinning at the magic angle during t_2.[16d] The use of MASSLF methods for spectral assignment as described here takes advantage of the fact that variations in the MASSLF dipolar sideband patterns due to subtle changes in geometry are insignificant when compared to the differences between patterns for carbons with different multiplicities. Methylenes, methines, and rapidly rotating methyls and nonprotonated carbons all have characteristic dipolar coupled patterns which can be used to separate and quantitatively determine the amounts of these types of carbons in a complex spectrum. This MASSLF method as described here has several advantages over the other solid-state spectral assignment techniques mentioned above. First, all carbon resonances are observed in one experiment facilitating direct comprison of the relative number of carbon types. This is to be contrasted with interrupted decoupling methods which require subtraction of two different spectra with an empirical correction factor to compensate for intensity differences. Another advantage of this method over interrupted decoupling is that it easily discriminates between methylenes and methines. In comparison to the 2D heteronuclear-shift experiment, the requirements for the quality of the proton homonuclear decoupling are somewhat relaxed since proton chemical shifts are not being measured. Imperfections in the multiple pulse decoupling will primarily affect the line widths and scaling factors of the observed sideband patterns and to a much lesser extent their form.

The assignment of ^{13}C CPMAS spectra using MASSLF techniques is demonstrated here for a polymer and a small biomolecule. The results indicate that the use of the MASSLF experiment for spectral assignment is no less quantitative then CPMAS spectroscopy itself, and it is expected that the method will find many uses in the assignment of complex ^{13}C CPMAS spectra.

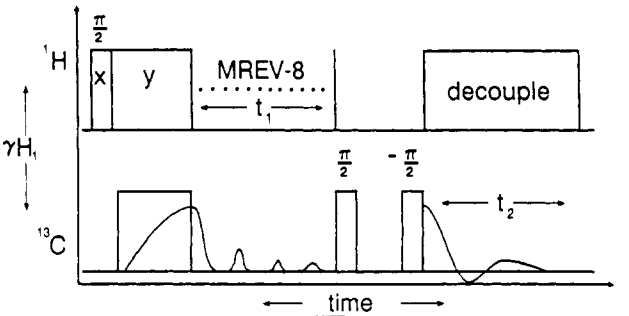

Figure 1. Pulse sequence used here for acquiring 2D MASSLF spectra. ^{13}C magnetization formed during cross polarization is allowed to evolve for a variable time t_1 with homonuclear decoupling of the protons. Typically an MREV-8 sequence in the semiwindowless limit is used. Evolution in t_1 is projected onto a single axis in the rotating frame by application of a pair of $\pi/2$ pulses separated either by a period of no decoupling or a homospoil pulse. A normal proton-decoupled ^{13}C FID is acquired in t_2 following application of the final $\pi/2$ pulse. The first $\pi/2$ pulse is incremented in phase by 90° for each successive point acquired in t_1 to produce the effect of a resonance offset in f_1.

Theory

General. The theory underlying the MASSLF method has been treated in detail elsewhere;[13,20,32,33] only those points relevant to the present method will be discussed. The basic idea in the application of MASSLF outlined here is that methylenes, methines, and methyls or nonprotonated carbons each give different and characteristic dipolar patterns in a 2D MASSLF spectrum. This statement is not meant to imply that different methines all have exactly the same dipolar sideband pattern; rather, the differences that can be observed are typically insignificant in comparison to the difference between a typical methine and a methylene.

In a typical experiment the spins are manipulated using a pulse sequence as illustrated in Figure 1. Following a period of cross polarization the ^{13}C magnetization evolves during t_1 under the influence of proton homonuclear decoupling. As discussed by previous workers this serves to render the ^{13}C–^{1}H heteronuclear dipolar interaction inhomogeneous.[16,20] The ^{13}C nuclei experience a local field which is the combined effect of the ^{13}C CSA and any heteronuclear dipolar interactions. During t_2 a standard proton-decoupled ^{13}C spectrum is acquired which is correlated to the evolution under the ^{13}C–^{1}H dipolar interaction in t_1. Since the ^{1}H–^{1}H homonuclear decoupling is eliminated, the effective Hamiltonian during t_1 for a general AX_n system then can be written as

$$\mathcal{H}(\Omega(t_1)) = -\mathbf{r}^{\mathrm{T}}\cdot\boldsymbol{\nu}\cdot\mathbf{r}\,S_z + \sum_{i=1}^{n}\mathbf{r}^{\mathrm{T}}\cdot\mathbf{R}_i\cdot\mathbf{D}_i\cdot\mathbf{R}_i^{\mathrm{T}}\cdot\mathbf{r}\,S_z I_{z,i} \qquad (1)$$

in frequency units with $\Omega(t_1)$ signifying the parametric dependence of $\mathcal{H}$ on time induced by the MAS rotation. In this equation ν is the chemical shift tensor of the observed A nucleus in its principal axis system in frequency units. The $\mathbf{D}_i$ are given by

$$\mathbf{D}_i = (\mathrm{sf})\frac{\hbar\gamma_A\gamma_X}{2\pi r_i^3}\begin{bmatrix}1 & & \\ & 1 & \\ & & -2\end{bmatrix} \qquad (2)$$

where r_i is the internuclear distance between the A nucleus and the ith X nucleus, and sf is the scaling factor of the homonuclear decoupling sequence. The unit vector r and its transpose $\mathbf{r}^{\mathrm{T}}$ give the direction of the static field in the CSA principal axis system. The $\mathbf{R}_i$ are the rotation matrices that bring the ith dipolar tensor into the CSA principal axis system. Using this form for the effective Hamiltonian it can be shown[34] for each possible combination of X nucleus spin states that the allowed A spin transitions

(19) Zilm, K. W.; Webb, G. G. *Fuel* **1986**, *65*, 721–724.
(20) Munowitz, M. G.; Griffin, R. G. *J. Chem. Phys.* **1982**, *76*, 2848–2858.
(21) Schaefer, J.; McKay, R. A.; Stejskal, E. O.; Dixon, W. T. *J. Magn. Reson.* **1983**, *52*, 123–129.
(22) Aue, W. P.; Ruben, D. J.; Griffin, R. G. *J. Magn. Reson.* **1981**, *43*, 472–477.
(23) Hester, R. K.; Ackerman, J. L.; Neff, B. L.; Waugh, J. S. *Phys. Rev. Lett.* **1976**, *36*, 1081–1083.
(24) DiVerdi, J. A.; Opella, S. J. *J. Am. Chem. Soc.* **1982**, *104*, 1761–1762.
(25) Roberts, J. E.; Harbison, G. S.; Munowitz, M. G.; Herzfeld, J.; Griffin, R. G. *J. Am. Chem. Soc.* **1987**, *109*, 4163–4169.
(26) (a) Opella, J. S.; Waugh, J. S. *J. Chem. Phys.* **1977**, *66*, 4919–4924. (b) Linder, M.; Hohener, A.; Ernst, R. R. *J. Chem. Phys.* **1980**, *73*, 4959–4970.
(27) Stoll, M. E.; Vega, A. J.; Vaughn, R. W. *J. Chem. Phys.* **1976**, *65*, 4093–4098.
(28) Frey, M. H.; DiVerdi, J. A.; Opella, S. J. *J. Am. Chem. Soc.* **1985**, *107*, 7311–7315.
(29) Schaefer, J.; Stejskal, E. O.; McKay, R. A. *J. Magn. Reson.* **1984**, *57*, 85–92.
(30) Schaefer, J.; Sefcik, M. D.; Stejskal, E. O.; McKay, R. A.; Dixon, W. T.; Cais, R. E. *Macromolecules* **1984**, *17*, 1107–1118.
(31) Schaefer, J.; Stejskal, E. O.; McKay, R. A.; Dixon, W. T. *Macromolecules* **1984**, *17*, 1479–1489.
(32) Herzfeld, J.; Roberts, J. E.; Griffin, R. G. *J. Chem. Phys.* **1987**, *86*, 597–802.
(33) Munowitz, M. G.; Griffin, R. G. *J. Chem. Phys.* **1983**, *78*, 613–617.
(34) Zilm, K. W.; Grant, D. M. *J. Am. Chem. Soc.* **1981**, *103*, 2913–2922.

can each be described by individual effective "chemical shift" tensors

$$\nu_{\mathrm{eff},j} = \nu - \sum_{i=1}^{n} m_{i,j}\mathbf{R}_i\cdot\mathbf{D}_i\cdot\mathbf{R}_i^{\mathrm{T}} \qquad (3)$$

where $m_{i,j}$ refers to the spin state of the ith X nucleus in the jth transition. This tensor is symmetric and therefore can always be diagonalized to form a new tensor $\mathbf{T}_j$ with only three components. Thus each of the 2^n A spin transitions can be treated as though they were due to 2^n individual CSA tensors with three principal components. If the spins are directly observed during an interval of proton homonuclear decoupling, i.e., in a one-dimensional MASSLF experiment, the sideband patterns observed will be given by the sum of the sideband patterns generated by the individual $\mathbf{T}_j$. This approach greatly simplifies the calculation as it is now identical with that originally proposed by Herzfeld and Berger for the case of CSA only.[32,35] The analysis is just as simple in a full two-dimensional MASSLF experiment as long as the MAS spin rate is sufficient to remove any CSA sidebands from the spectra observed in f_2. When the MAS rate ν_r is slow compared to the CSA, the analysis is more complex and has been treated elsewhere.[13,20,32] MASSLF 2D spectra under these conditions are quite sensitive to the relative orientations of the dipolar and chemical shift tensors. For the purpose of spectral assignment this presents an additional complication that is to be avoided, and it is assumed in what follows that no sidebands appear in the spectra acquired in f_2.

The evolution in t_1 is indirectly detected in a full 2D experiment. In other versions of the MASSLF method, evolution in t_1 under the isotropic shift is removed by application of a π pulse at the peak of a rotational echo.[13,21,22] The effects of the anisotropic chemical shift are likewise suppressed by commencing data acquisition (t_2) at an integral number of rotor cycles from the beginning of t_1. Such precautions are necessary if the sideband patterns in f_1 are to be free of chemical shift effects. For the purpose of spectral assignment this is not strictly required (vide infra) as long as the dipolar interactions are many times larger than the CSA. This is the case at field strengths the order of the 2.35 T used here, and in this instance the simpler pulse sequence in Figure 1 can be employed. For the purpose of the present discussion the effects of chemical shift will then be assumed minor or that a sequence has been employed to remove them altogether. The sideband patterns observed in f_2 therefore can be calculated from eq 3 for $\nu_{\mathrm{eff},j}$ setting ν to zero. The remaining term depends on the number of protons attached to a particular carbon and the values of the C–H bond distances, r_i, and any H–C–H angles. Previous work has focussed almost exclusively on the sensitivity of the MASSLF patterns to the r_i by virtue of the $\langle 1/r_i^3\rangle$ dependence of the dipolar couplings. While the patterns are, in fact, sensitive to small variations in structure, the dependence on the number of couplings is a much greater effect. This is demonstrated in Figure 2 which shows a typical CH_2 pattern to be about $2^{1/2}$ times wider than a CH pattern, and that both are quite different from those for nonprotonated and methyl carbons. Since methyls rapidly rotate about their pseudothreefold axis, under most conditions their time-averaged C–H dipolar couplings are quite small. Operationally they will be considered the same as nonprotonated carbons in what follows. These differences in the dipolar patterns will be used as a basis for separately accounting for the three types of carbons. Since the variation in MASSLF patterns is more a function of multiplicity than geometry, standard sets of ν_j can be arrived at for each multiplicity and used to calculate the MASSLF patterns for a particular ν_r and scaling factor.

Spectral Assignment. Given that a set of characteristic MASSLF patterns can be calculated for a particular ν_r, assuming representative geometries and no large amplitude molecular motion other than methyl rotation, the assignment of a relatively complex CPMAS spectrum is straightforward. The most ideal method would be to use the calculated sideband intensity ratios to deconvolve the chemical shift spectrum into separate methylene, methine, and methyl plus nonprotonated spectra. This approach does, however, require a rather high signal-to-noise ratio as the noise level in the reconstructed spectra will largely be determined by the signal to noise in the outermost sidebands. In practice a much simpler analysis is possible using dipolar slices parallel to f_1. To determine the multiplicity of a particular ^{13}C resonance, the f_1 slice at that position is compared with the set of standard sideband intensities for the conditions used. In cases where there is not spectral overlap in f_2, assignment is simple and can be done on inspection. If overlap is severe the analysis is still relatively easy. The experimental sideband intensities can be represented by a vector I with components I_i for each of the $\pm i$th sidebands. To determine the relative number of different contributing carbon types, the linear combination of the characteristic intensity vectors $I_{n,i}$ must be found for each sideband. That is, the experimental vector I_i can be written as

$$I_i = \sum_n \alpha_n I_{n,i} \qquad (4)$$

The α_n are the fractions of the three types of carbons contributing to the resonance in question. Since there will usually be at least four sets of sidebands, the α_n are overdetermined, giving an internal consistency check.

One way to determine the α_n's would be to simulate the MASSLF spectra using the standard patterns in an iterative process. A better approach would entail computer solution of the eq 4 and minimization of the variance. Because there will usually be a number of solutions (α_n) to the set of equations for a given experimental spectrum, a graphical technique has been employed which displays the scatter in the set of solutions more clearly than computer methods and is less time consuming than trial and error simulations. Since rapidly rotating methyl and nonprotonated carbon dipolar sideband patterns are nearly indistinguishable, the maximum number of n in most cases will be three. The case of n equal to two is conceptually the simplest to consider. The solutions for the α_n will be represented by the intersections of the lines given by:

$$I_i = \alpha_1 I_{1,i} + \alpha_2 I_{2,i} \qquad (5)$$

for each sideband plotted in the α_1,α_2 coordinate system and the constraint $\alpha_1 + \alpha_2 = 1$. Other possible solutions will be represented as intersections of the sideband lines with each other. As there will be some error in the model and experimental intensities, these points will not necessarily fall on the constraining line. These intersection points can then be scaled to give the α_n.

For three unknown α_n the graphical method is similar. Now each sideband in the experimental spectrum will generate a plane

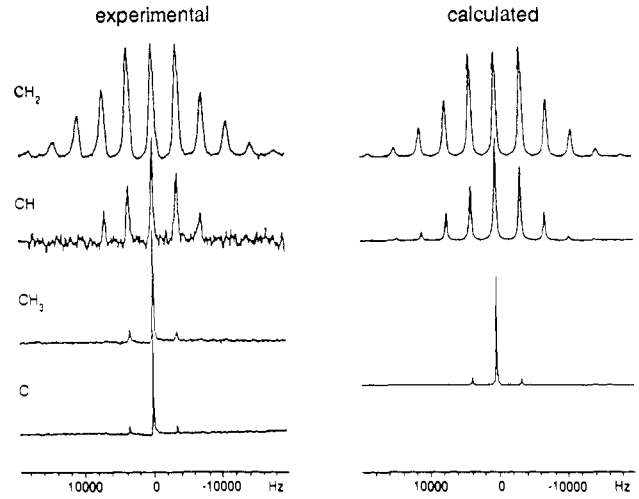

Figure 2. Typical MASSLF patterns observed at 2.35 T and spin rates ~3.5 kHz. The CH_2 pattern is from paraformaldehyde, the others are taken from a 2D MASSLF spectrum of dimethoxybenzene. Simulations using the proposed standard dipolar plus CSA tensors are provided for comparison. Note that the line widths in the MASSLF patterns are greater the more protons are attached to a given ^{13}C center.

(35) Herzfeld, J.; Berger, A. E. *J. Chem. Phys.* **1980**, *73*, 6021–6030.

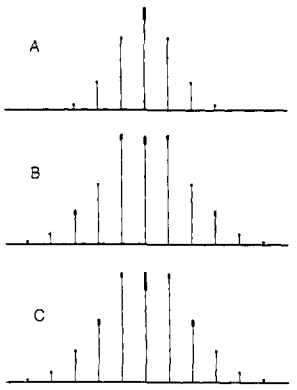

Figure 3. (A) Stick MASSLF spectrum at ν_r = 3.5 kHz for a methine using a range of r_{CH} values assuming no CSA contribution. The thick portion of each line indicates the variation in intensity for r_{CH} between 1.08 and 1.10 Å. The values for r_{CH} = 1.09 Å are approximately midway between the end points. For lines topped by a • the range is too small to accurately portray on this scale. In no case is the variation more than ±5%. All calculated spectra included in this plot were scaled to have the same integrated intensity. (B) The same as A but for a CH_2 group with the H-C-H angle fixed to 109.46°. (C) Changes in the MASSLF patterns for a methylene as the H-C-H angle is varied over a small range. r_{CH} = 1.09 Å and the H-C-H angle is varied ±5° about the tetrahedral angle. The largest intensity variation is the ±7% calculated for the center band. The pattern for the other lines is essentially the same for all angles in this range. Tables of the calculated sideband intensities used to construct this figure are available in the supplementary material.

in the α_1, α_2, α_3 coordinate system. The solution points will be constrained to the first octant on the plane $\alpha_1 + \alpha_2 + \alpha_3 = 1$. The best way to represent the possible solutions is to plot the intersections of the sideband plane equations with the constraining plane as lines on the surface of an equilateral triangle. The triangle represents the area of the constraining plane in the first octant. The intersections of these lines on the triangle give a set of solution points for the experimental sideband pattern.

Limitations. The above method of analysis assumes that the variations in MASSLF patterns associated with reasonable variations in geometry are so small that they may be ignored for the purpose of distinguishing the three types of carbon centers. That this is indeed the case is demonstrated by the calculated sideband intensities contained in Figure 3 for methylenes and methines using a range of C-H distances and H-C-H angles, spinning at 3.5 kHz. The variations under the assumed experimental conditions are seen to be only a few percent and very much less than the differences between the two types of patterns. These results are not to be taken as contrary to previous work which demonstrated the sensitivity of MASSLF patterns to C-H distances and geometry. Other workers have used much higher field strengths and slower spin rates which produce patterns more sensitive to geometry and CSA. The assumption of limited molecular motion also somewhat restricts the applicability of this method. The presence of large amplitude motions will introduce errors in the analysis of spectra using the assumptions applied here. However, such motions may often be frozen out using low-temperature operation. As to be discussed later, ultra-high-frequency low-amplitude motions apparently do not adversely affect the results of this type of analysis. Additionally, the method here will be limited by the same error present in any CP experiment, that of unequal transfer of polarization to all types of carbons.[36,37]

The validity of using a single calculated standard sideband pattern to experimentally fit all carbons of any one type is not solely a question of how small a range may be expected in C-H distances and H-C-H angles in organic solids. Experimentally the MASSLF patterns for CH and CH_2 groups (assuming an

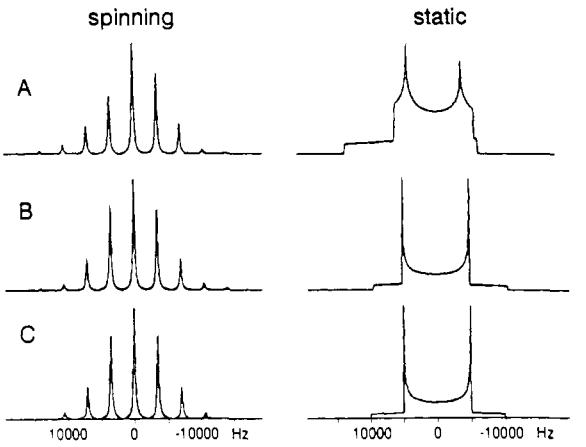

Figure 4. MASSLF patterns and static powder patterns for a methine with and without CSA: (A) using a CSA appropriate for an aromatic CH; (B) using a CSA appropriate for an aliphatic CH; (C) using no CSA. If the ±n sidebands are averaged, the effects of CSA are largely suppressed (see Table I).

H-C-H angle) only determine the ratio of D_{eff}/ν_r where D_{eff} is given by:

$$D_{eff} = (\hbar\gamma_H\gamma_C/2\pi r_{CH}^3)sf \quad (6)$$

Thus the patterns observed in the 2D MASSLF method are also dependent upon ν_r and the sf as well as the value of $\langle 1/r^3 \rangle$. Sideband intensities for both CH and CH_2 groups are provided for a wide range of D_{eff}/ν_r in Tables I-VII of the supplementary material. If the actual C-H distance deviates by 0.01 Å from an assumed standard value of 1.09 Å, the assumed D_{eff} will be in error by ~300 Hz and the real D_{eff}/ν_r value will differ by 0.07 at ν_r = 3.5 kHz and using the sf for MREV-8. Alternatively the same error in the D_{eff}/ν_r ratio could be the result of the sf being off by 0.01. An error in the D_{eff}/ν_r ratio could also be taken as an error in the spinning speed. At the spinning speed of 3.50 kHz, an error of 0.07 in D_{eff}/ν_r is equivalent to an error of 100 Hz in the spinning speed. Thus if the sf is not known to any more precision than 0.018 or the spin rate is uncertain by 100 Hz, the value of r will have an uncertainity of ~0.01 Å. For the purpose of using MASSLF patterns in spectral assignment, this means that the errors produced by assuming a single C-H distance of 1.09 Å, when actual distances may typically vary ±0.01 Å from this, are comparable to having an error of 0.01 in sf or 100 Hz in the spin rate. As long as the standard r used is the median value expected, the effects of small variations in C-H bond length will tend to average themselves out (see Figure 3). In going from sp^3 to sp^2 to sp carbons the C-H bond length is expected to become progressively shorter. Since these types of carbons also have different ranges of ^{13}C chemical shifts, a different standard r may be assumed for each shift range separately without complicating the analysis. Thus a value of 1.09 Å might be appropriate for aliphatic carbons, while a value of 1.08 Å may produce better results for aromatics.

For methylenes the variation in H-C-H angle must also be considered (Figure 3C). A variation of ±5° in the H-C-H angle about the tetrahedral angle produces variations in the normalized sideband patterns comparable to those resulting from a ±0.01 Å variation in r. From the list of methylene sideband intensities in Table VII of the supplementary materials, it can be seen that the variations are most pronounced in the first sideband and further that these changes are not consistent with changes in the ratio of D_{eff}/ν_r. The patterns calculated for an H-C-H angle of 120°, as expected for a vinyl CH_2 group, are very different from those calculated using 109.46°. Therefore, just as a somewhat shorter C-H distance should be used for the aromatic portion of the ^{13}C spectrum than used in the aliphatic part, the H-C-H angle used should be appropriate for the hybridization of carbon as well.

Inclusion of CSA. At the expense of a somewhat more complex experimental setup, the limitations of the analysis can be kept to those discussed above. However, comparable results can be ob-

(36) Alemany, L. B.; Grant, D. M.; Pugmire, R. J.; Alger, T. D.; Zilm, K. W. *J. Am. Chem. Soc.* **1983**, *105*, 2133-2141.
(37) Alemany, L. B.; Grant, D. M.; Pugmire, R. J.; Alger, T. D.; Zilm, K. W. *J. Am. Chem. Soc.* **1983**, *105*, 2142-2147.
(38) Rhim, W.-K.; Elleman, D. D.; Vaughan, R. W. *J. Chem. Phys.* **1973**, *59*, 3740-3749.

Table I. Comparison of Symmetrized Sideband Intensities in Methines and Methylenes[a]

Methine $\Delta D = 2D_{eff} = 20058$ Hz

	$\nu_r = 3.5$ kHz				$\nu_r = 5.5$ kHz	
ss no.	no CSA	aliphatic CSA	aromatic CSA	aromatic CSA*	no CSA	aromatic CSA
±6	0.0003	0.0002	0.0006	0.0005		
±5	0.0018	0.0018	0.0030	0.0028	0.0001	0.0001
±4	0.0130	0.0132	0.0166	0.0163	0.0008	0.0012
±3	0.0540	0.0540	0.0582	0.0604	0.0060	0.0076
±2	0.2816	0.2808	0.2630	0.2692	0.0546	0.0593
±1	0.7463	0.7412	0.6205	0.6495	0.2588	0.2552
0	1.0000	1.0000	1.0000	1.0000	1.0000	1.0000
$\Delta\nu$(Hz)	0	628	4451	4451	0	4451
$\Delta\nu/\nu_r$	0	0.18	1.3	1.3	0	0.81
$\Delta D/\Delta\nu$		31.9	4.51	4.51		4.51
$\Delta D/\nu_r$	5.7	5.7	5.7	5.7	3.6	3.6
std dev		0.0023	0.0569	0.0483		0.0031

Methylene $\theta_{HCH} = 109.46°$, $\Delta D = 2\sqrt{2}D_{eff} = 28366$ Hz

	$\nu_r = 3.5$ kHz					$\nu_r = 5.5$ kHz	
ss no.	no CSA	PF CSA	PF CSA*	ethylene CSA*	ethylene CSA#	no CSA	ethylene CSA*
±7	0.0009	0.0008	0.0008	0.0010	0.0012		
±6	0.0048	0.0048	0.0049	0.0056	0.0060		
±5	0.0237	0.0238	0.0240	0.0254	0.0276	0.0009	0.0011
±4	0.0914	0.0914	0.0920	0.0919	0.1014	0.0059	0.0072
±3	0.3025	0.3006	0.3022	0.2730	0.3006	0.0387	0.0419
±2	0.5763	0.5720	0.5792	0.5132	0.6286	0.1608	0.1694
±1	1.0442	1.0302	1.0412	0.8352	1.0023	0.5271	0.5134
0	1.0000	1.0000	1.0000	1.0000	1.0000	1.0000	1.0000
$\Delta\nu$(Hz)	0	1250	1250	5282	5282	0	5282
$\Delta\nu/\nu_r$	0	0.36	0.36	1.5	1.5	0	0.96
$\Delta D/\Delta\nu$		22.7	22.7	5.37	5.37		5.37
$\Delta D/\nu_r$	8.1	8.1	8.1	8.1	8.1	5.2	5.2
std dev		0.0060	0.0017	0.0899	0.0277		0.0083

[a] All orientations are those of the model tensors except when marked with *'s and #'s. The * methine has the C-H vector parallel to the high-frequency CSA component. In the * PF (paraformaldehyde) the high-frequency CSA component bisects the H-C-H angle, and the low-frequency component is perpendicular to the H-C-H plane. The * ethylene CSA consists of ethylene CSA components in the assumed PF orientation (see text). The # ethylene CSA consists of ethylene CSA components in the * PF orientation.

tained with the asynchronous MASSLF pulse sequence depicted in Figure 1. The principal difference between this sequence and other versions is that the effects of chemical shift are not removed in t_1. This poses no particular difficulty as it can be shown that at moderate field strengths (2.35 T) and using moderately fast MAS rates, ~3 kHz, the effects of the CSA on the sideband patterns is quite small. In Figures 4 and 5 are shown comparisons of the calculated full powder patterns and sideband patterns for a methylene and a methine with and without CSA and for various orientations of the dipolar tensors with respect to the CSA principal axis system. While the features present in the powder patterns are quite sensitive to the magnitude of the CSA and the relative orientations of the pertinent tensors, these effects are practically washed out when the MAS spin rate exceeds the width of the CSA in frequency units. Features resolvable in the powder spectrum, separated by frequencies the order of the MAS spin rate or less, are effectively mixed together and not resolved in the MAS spectrum as shown in these figures. The main effect of the inclusion of the CSA is to produce an asymmetry in the sideband patterns. This suggests that much of the effect of CSA can be removed by averaging the $\pm n$ sideband intensities. The set of methylene and methine calculated sideband intensities in Table I demonstrates that symmetrizing the intensities does indeed nearly remove the effects of the CSA. The symmetrized sideband intensities with CSA are very close to those from a calculation without CSA included. This assumption becomes less valid as the spinning frequency is decreased, with the deviations first occurring at the sidebands closest to the centerband.

Looking at Table I, for a methine the effect of a large CSA on the sideband intensities is most severe. This is expected as the dipolar breadth for a methine ($2D_{eff}$) is a factor of $2^{1/2}$ smaller than for a methylene. For an aliphatic CSA of around 600 Hz, the dipolar breadth to CSA ratio is 32.9. For an aromatic CSA of 4500 Hz, the methine dipolar breadth to CSA ratio is 4.5, an order of magnitude smaller than that for the aliphatic CSA. The

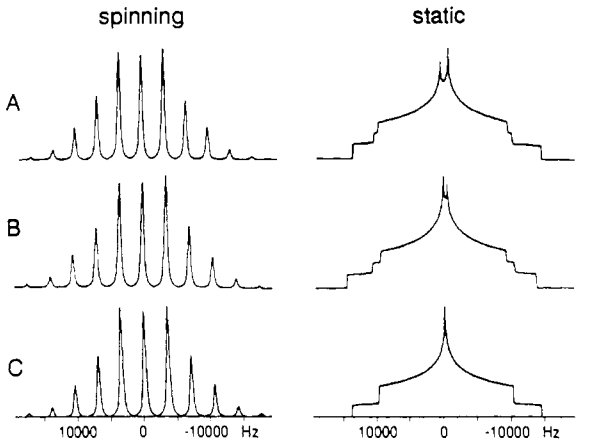

Figure 5. MASSLF patterns and static powder patterns for a methylene with and without CSA. (A and B) Using the CSA for paraformaldehyde. In B the assumed orientation of the CSA with respect to the H-C-H plane is used. In A the CSA axis have been permuted as noted in Table I. While the static patterns are sensitive to the orientation of the CSA, the MASSLF patterns are not under these conditions. (C) Pattern without any CSA. Note that all three MASSLF patterns are essentially identical.

standard deviation between the intensities of the simulated sidebands with and without CSA gives a quantitative idea of the discrepancies. When the spinning speed is increased to 5.50 kHz, the standard deviation decreases by an order of magnitude. Similar behavior is observed for the methylene case given in Table I, and is also observed for vinyl carbons (see Table VI of the supplementary materials). These numbers demonstrate that in the aliphatic region of the spectrum the symmetrized sideband intensities approximate those without CSA quite well. In the aromatic region the symmetrized sideband intensities are close

but do not agree as well. Looking at specific sidebands within the symmetrized set, the most deviation occurs at the first sideband.

Errors in the CSA orientation have little effect on the sideband intensities. For the aromatic methine CSA and the methylene CSA different orientations were chosen to compare the resulting intensities. In all cases most of the variation occurred at the first sideband, and the standard deviation from the no CSA intensities was within an order of magnitude for all orientations. The effects of a different orientation are also minimized as the MAS rate increases. The change in the CSA orientation has the most effect on patterns with a D_{eff} to CSA ratio below 10. From these computer simulations it can be concluded that in the aliphatic portion of the ^{13}C chemical shift range, where the CSA's are relatively small, the effects of the CSA and uncertainties in its exact value and orientation can be removed by averaging or symmetrizing the sideband intensities. In regions of the spectrum with larger CSA's, the agreement will be better at relatively rapid spin rates, and the first sideband intensity will have more uncertainty than the others will have. It is important to note that the cases with a D_{eff} to CSA ratio below 10 will usually be aromatic methines, and the orientation and size of the CSA are fairly uniform for this type of carbon.

In general most of the effect of CSA can be included in the standard ν by choosing representative CSA's for the different types of carbons. In the aliphatic region no CSA is really required at all, but inclusion of a small CSA the order of 30–50 ppm will often give minor improvement in the agreement between the standard MASSLF pattern and those observed for typical aliphatic groups. In the aromatic region the inclusion of a CSA the order of 200 ppm gives a significant improvement in the degree to which a standard set of sideband intensities will simulate those for a typical aromatic methine or vinyl carbon.

Asynchronous MASSLF. For the purpose of spectral assignment, the suppression of chemical shifts in t_1 is not necessary, and this simplifies the experimental setup as a MAS speed controller is not required. In the MASSLF pulse sequence used here, the transverse ^{13}C magnetization is simply projected onto one axis of the rotating frame at the end of t_1. This can be accomplished by applying a $\pi/2(\phi)-\tau-\pi/2(-\phi)$ sequence in which the time τ is a homospoil period or a period of interrupted decoupling to dephase any transverse magnetization during τ. After the projection step, the ^{13}C magnetization is detected with strong resonant proton decoupling giving a 2D data set of heteronuclear dipolar/CSA sideband patterns correlated to ^{13}C isotropic chemical shifts.

This particular sequence has several advantages for the purpose at hand. Since synchronization with the MAS rotation is not required, implementation of the pulse timing program is straightforward. Phase twist[39] is not a problem with this sequence as the projection step produces a purely amplitude modulated data set. Quadrature detection in t_1 can be simulated by using time proportional phase incrementation (TPPI)[40] to sequentially advance the phase of the projection step pulse by 90° for each value of t_1. This results in the carrier frequency in f_1 appearing at one extreme edge of the f_1 spectrum when it is actually placed in the center. Other MASSLF sequences are constant time experiments in the sense that data acquisition in t_2 is always postponed from the beginning of t_1 by a time n/ν_r corresponding to the longest value of t_1. This is done in order to suppress the effects of the anisotropic portion of the chemical shift in f_1. With the sequence employed here, data are acquired almost immediately after the multiple pulse decoupling period resulting in an often considerable gain in sensitivity over a constant time experiment.

It has also been found that this sequence permits the large bandwidth needed in f_1 to observe the broad patterns characteristic of methylenes as the homonuclear decoupling can be conveniently incremented in subdivisions of t_c. One might suppose that in MASSLF experiments observation of the carbon magnetization in t_1 must coincide with the homonuclear decoupling cycle and that at least one full cycle of multiple pulse decoupling be applied before the protons can be considered decoupled. However, this is never the case as long as the homonuclear decoupling is operated in the *average Hamiltonian limit*. In this limit the carbon magnetization behaves as if it sees a dipolar field due to the protons that is quite the same as if the proton–proton dipolar couplings were in fact zero at *all* times, not just on the average at multiples of the cycle time. This is because, in the average Hamiltonian limit, the phase angle actually accumulated by the spins converges upon that which would be found if the Hamiltonian were indeed the average Hamiltonian. In other words, the magnetization closely follows an evolution described by the average Hamiltonian at all times; there are not wild variations in accumulated phase. The worst that can happen then is that there will be very small periodic departures of the magnetization from the evolution described by the average Hamiltonian. The only effect of such departures will be to produce rather weak sidebands at frequencies that are multiples of $1/t_c$ in the dipolar slices.

Experimental Section

All experiments were performed on a homebuilt NMR spectrometer based on a Nicolet 1280 data system and using an Oxford Instruments 2.35-T, 110-mm room-temperature bore superconducting solenoid. The radio frequency (rf) electronics are similar to those described in ref 41 and 42. Spectra were acquired using a CPMAS probe utilizing a double bearing MAS turbine and 9-mm boron nitride rotors. A unique feature of this probe is that it incorporates a continuously variable pitch rf coil designed to optimize the rf field for the homonuclear decoupling.[43] Proton $\pi/2$ pulse times and phase angles were set using a small spherical sample of 1 mM $MnCl_2$ doped water. The proton reflected power was kept near minimum during this setup, as well as throughout the 2D run to ensure a consistent performance of the multiple pulse decoupling sequence. The multiple pulse scaling factor was determined prior to the two-dimensional experiment, and checked again after the completion of the run. This experimental scaling factor was the value used in all sideband simulations done for the analysis of spectra of this 2D run.

Spectra of ^{13}C-enriched paraformaldehyde were used to determine the effective MREV-8 scaling factor. These were taken using the semiwindowless MREV sequence[16,44] applied after the Hartmann–Hahn match in the standard CPMAS pulse sequence. The breadth of the MREV-8 scaled dipolar sideband pattern necessitated the use of a Hahn echo,[45] keeping τ either much less than or equal to the MAS rotor period.

In a typical 2D experiment MREV-8 decoupling in the semiwindowless limit has been used. During t_1 the decoupling was incremented in 3τ portions of the 12τ MREV-8 cycle time. Typical $\pi/2$ proton pulses were 3.5 to 4.0 μs, and the Hartmann–Hahn matched cross polarization was performed at $\gamma H_1/2\pi$ = 63 kHz. Artifacts produced by pulse imperfections in the projection step were very effectively suppressed by phase cycling the cross polarization mixing pulse together with spin temperature inversion.[46,47] Typical acquisition times for the 2D data sets reported here ranged from 2 to 10 h. No attempts have been made to regulate the MAS spin rate other than using several stages of regulation on the high-pressure air source. This has been found sufficient to ensure no more than a 20-Hz variation while running at rates of 3 to 4 kHz.

In all 2D experiments after the initial Fourier transform and phasing of the data, the imaginary portion of each spectrum was set to zero before the transposition and the final transform. These manipulations and the data acquisition cannot be conveniently accomplished without modification of the standard Nicolet software package. The necessary software for these modifications was supplied by Dr. Andrew Byrd. Simulations of all sideband spectra were done on a VAX/11-750 using the same algorithm as outlined by Herzfeld and Berger. Consistency of the sideband spectra was checked by comparison of results from our program to outputs kindly supplied by Dr. A. E. Berger and Dr. R. G. Griffin.

(39) Bax, A. *Two Dimensional Nuclear Magnetic Resonance Spectroscopy in Liquids*; D. Reidel: Dordrecht, The Netherlands, 1982.
(40) Bodenhausen, G.; Freeman, R.; Morris, G. A.; Niedermeyer, R.; Turner, D. L. *J. Magn. Reson.* **1977**, *25*, 559–562.
(41) Gross, S.; Zumbulyadis, N. *Rev. Sci. Instrum.* **1982**, *53*, 615–623.
(42) Bartuska, V. J.; Maciel, G. E. *J. Magn. Reson.* **1981**, *42*, 312–321.
(43) Idziak, S.; Haeberlen, U. *J. Magn. Reson.* **1982**, *50*, 281–288.
(44) Burum, D. P.; Linder, M.; Ernst, R. R. *J. Magn. Reson.* **1981**, *44*, 173–188.
(45) Abragam, A. *Principles of Nuclear Magnetism*; Oxford University Press: New York, 1983; p 58.
(46) Stejskal, E. O.; Schaefer, J. *J. Magn. Reson.* **1974**, *14*, 160–164.
(47) Stejskal, E. O.; Schaefer, J. *J. Magn. Reson.* **1975**, *18*, 560–563.

Table II. Comparison of Experimental Paraformaldehyde and Calculated Best Fit Methylene with No CSA Sideband Intensities, Scaled to ±1st Sideband

ss	exptl ν_r(kHz)			
no.	3.42	3.04	2.52	2.18
±8				
±7				
±6				0.12
±5		0.06	0.16	0.28
±4	0.09	0.16	0.37	0.50
±3	0.30	0.42	0.61	0.61
±2	0.56	0.64	0.69	0.68
±1	1.00	1.00	1.00	1.00
0	0.94	1.00	1.19	1.26
ss	calcd D_{eff}/ν_r			
no.	2.87	3.28	4.00	4.60
±8				
±7				
±6				0.13
±5		0.05	0.16	0.29
±4	0.09	0.16	0.36	0.53
±3	0.29	0.42	0.62	0.69
±2	0.55	0.64	0.71	0.73
±1	1.00	1.00	1.00	1.00
0	0.96	0.96	1.07	1.16
SF[a]	0.42	0.43	0.43	0.43

[a] SF = $[(D_{eff}/\nu_r)\nu_r]/D$, where D = 23322 Hz, for r_{CH} = 1.09 Å.

The scaling factor was determined by comparing the symmetrized experimental paraformaldehyde sideband intensities with tables of calculated, symmetrized methylene sidebands listed by their D_{eff} to MAS rate ratio. A copy of this table is available in Table VII of the supplementary materials, part of which is reproduced in Table II. Using the experimentally determined scaling factor and the spinning speed, standard sideband intensities for methylene, aromatic methine, aliphatic methine, and methyl plus nonprotonated carbons were calculated. The model intensities used in the analysis were averaged and normalized to their sum to give the set of $I_{n,i}$ used in the sideband analysis. Where possible these model intensities were checked with experimental sideband patterns. It is important that the calculated sidebands be normalized to the sum of the same number of sidebands that are in the experimental spectrum and will be used in the analysis.

For the methines, the model tensors used in the analysis were obtained from literature CSA's and geometries. For the aromatic methine, durene was used,[48] and, for the aliphatic methine, bicyclo[1.1.1]pentane[49] was chosen. The model methylene was paraformaldehyde,[50] with an orientation placing the H-C-H plane perpendicular to the high-frequency component, ν_{11}, and ν_{22} bisecting the H-C-H angle. The vinyl CH_2 CSA was that of ethylene.[34] For methyl and nonprotonated carbons a single η = 1 tensor with a $\Delta\nu = \nu_{11} - \nu_{33}$ = 6400 Hz was chosen. This tensor was found to mimic both nonprotonated carbons and the more complex situation of the rapidly rotating methyl at the spinning speeds used.

Samples of 95% ^{13}C-enriched paraformaldehyde were used as received from Merck. Cholesteryl acetate (Aldrich), *p*-dimethoxybenzene (Aldrich), and 60% isotactic polystyrene (Polysciences) were also used as received.

Results and Discussion

Determination of the Scaling Factor. Typical MASSLF patterns for methylene, methine, methyl, and nonprotonated carbons are shown in Figure 2. The methylene pattern is from the sample of ^{13}C-enriched paraformaldehyde, and it is identical with the pattern observed simply by using homonuclear decoupling in an otherwise standard CPMAS experiment. The other three patterns are slices from an asynchronous MASSLF experiment on *p*-dimethoxybenzene. As shown in the figure the observed intensities are very close to the standard set calculated for this ν_r using a homonuclear scaling factor of 0.43. The most striking feature of these spectra is that the line widths are seen to depend strongly on the multiplicity of the carbon centers. This is undoubtedly due to imperfections in the homonuclear decoupling and may also be partially due to interference between the MAS rotation and the homonuclear decoupling process.

Looking at the comparison of experimental symmetrized paraformaldehyde intensities to intensities calculated without CSA in Table II at moderately fast MAS rates, the agreement is seen to be very good. Only at speeds below 2 kHz do significant disagreements occur. The digressions occur in the early sideband intensities. This behavior is consistent with a slight variation of the true geometry of the methylene group and the orientation of the CSA from the ideal geometry and orientation chosen as discussed previously. Neglecting the early sidebands, at the slower spinning speeds the effective scaling factor determined is always within the range of 0.43 ± 0.01. By comparing the intensities in Table VII of the supplementary material with those in Figure 3, small changes in the outer methylene sidebands due to a deviation of the angle by a degree could not be mistaken as a change in the scaling factor of any more than 0.01. For the purpose of determining the scaling factor from a methylene, variations greater than 1 or 2° from the assumed H-C-H angle will result in noticeably worse agreement with the tabulated sideband intensities, even at MAS rates of 3 to 4 kHz.

The observed scaling factor of 0.43 is somewhat less than the ideal (corrected for finite pulse width) value of 0.536 for the semiwindowless MREV-8 pulse sequence.[51] The deviation of the MREV-8 scaling factor from the ideal value has been discussed by other investigators.[25,30] Schaefer et al. observed a decrease in their WAHUHA ideal scaling factor by a similar amount.[30] When this semiwindowless decoupling sequence was used to observe the ^{13}C-^{1}H *J*-couplings in samples of liquid acetone (static) and solid adamantane (MAS), the scaling factor was determined to be 0.54 ± 0.01, which is in very good agreement with the ideal corrected value. Thus, the determination of the effective scaling factor to be used in the MASSLF sideband pattern simulations must be done from a sample with ^{13}C-^{1}H dipolar couplings, as opposed to one with ^{1}H chemical shifts or ^{13}C-^{1}H *J*-couplings. This dipolar coupling scaling factor can be thought of as an effective scaling factor which includes the effects of high-frequency vibrations that average the dipolar coupling.[25,30] That the difference between the sf's measured using a liquid sample and a C-H dipolar coupled sample is due to ubiquitous high-frequency lattice motions is supported by low-temperature experiments. The value of 0.43 has also been obtained on paraformaldehyde at 77 K. The same value has been measured for each carbon in 2-methyltetrahydrofuran at 77 K as well.[52] One could interpret this apparent reduction in the scaling factor as an indication that the C-H bond length is actually considerably longer than assumed. Whether or not this is the case is not at issue here. Our experiments indicate that the same reduction in the scaling factor is observed for a variety of chemical systems and over a wide range in temperature. Therefore, one can take the position that the reduction is due either to C-H bond distances being always longer[25] than the 1.09 Å assumed here or to high-frequency molecular or lattice motions[30] common to organic solids in general or both. For the purposes of our analysis, the important observation is that the effective scaling factor remains fairly constant from system to system.

Polystyrene. Polystyrene provides a good model system to test several aspects of this technique. In the ^{13}C CPMAS spectrum in Figure 6, the methine and methylene carbon resonances are almost coincidental. The only spectral clue that there might be two signals at this position is the asymmetry of the line shape due to the small chemical shift and line width differences of these two carbons. Also in this figure are sideband patterns obtained by summing MASSLF slices within the aliphatic and protonated aromatic peaks onto the f_1 axis. Corresponding simulated spectra are shown for comparison. The experimental aliphatic sideband pattern agrees well with a 1:1 sum of the characteristic patterns

(48) Pausak, S.; Pines, A.; Waugh, J. S. *J. Chem. Phys.* **1973**, *59*, 591-595.
(49) Facelli, J. C.; Orendt, A. M.; Solum, M. S.; Depke, G.; Grant, D. M.; Michl, J. *J. Am. Chem. Soc.* **1986**, *108*, 4268-4272.
(50) Veeman, W. S. *Prog. NMR Spectrosc.* **1984**, *16*, 193-235.
(51) Rhim, W.-K.; Elleman, D. D.; Vaughan, R. W. *J. Chem. Phys.* **1973**, *58*, 1772-1773.
(52) Zilm, K. W.; Merrill, R. A.; Webb, G. G.; Greenberg, M. M.; Berson, J. A. *J. Am. Chem. Soc.* **1989**, *111*, 1533-1535.

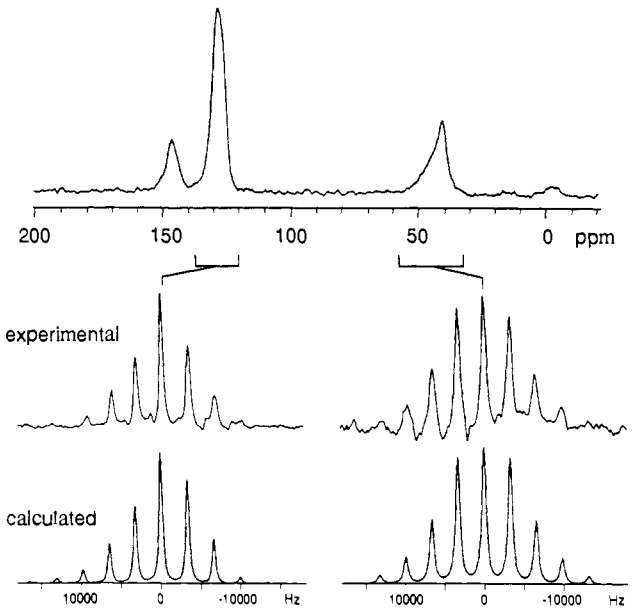

Figure 6. (Top) ^{13}C CPMAS spectrum of polystyrene; (middle) MASSLF patterns for the aliphatic and protonated aromatic resonances; (bottom) simulations of the experimental MASSLF patterns. Agreement of the relative integrated intensities is quite good. The small discrepencies in peak heights between experimental and calculated spectra are largely due to the fact that the simulations use the same line width for each sideband while the line widths are observed experimentally to increase as one moves out to progressively higher order sidebands.

for a methine and a methylene. In the aromatic pattern the experimental sideband line widths vary, making a comparison based on peak heights invalid. However, the experimental integrated intensities do agree well with model aromatic methine intensities. The presence of aromatic ring flips in a small fraction of the molecules apparently does not distort the pattern by a significant amount.[30] This is not to say that in all cases motions of this sort[31] will not have an effect on the analysis.

The next step in testing this assignment method is to use the model tensor intensities for methines and methylenes to determine their relative amounts in the aliphatic sideband pattern. Using symmetrized and normalized integrated peak intensities for the experimental spectrum, the α_{CH_2}, α_{CH} plot in Figure 7 shows the set of solutions for the aliphatic pattern. Note that the majority of the solutions cluster around the average value. The model tensor and experimental intensities used in the analysis appear in Table VIII of the supplementary materials. The results of this analysis, $(\alpha_{CH_2}, \alpha_{CH}) = (0.42, 0.58)$, gives a CH_2 to CH ratio of 0.8:1.2, which is in fairly good agreement with the known 1:1 ratio. The scatter of the points both on and off the constraining line leads to some uncertainty in the $(\alpha_{CH_2}, \alpha_{CH})$ average point. The coordinates of the solution points off the constraining line must be scaled so their ratio remains constant and they meet the condition that their sum is one. Looking at the scatter of solutions on the constraining line, the two outermost points are due to the centerband and first sideband. These sidebands are more susceptible to errors as discussed earlier. The outermost sideband will also be subject to more relative uncertainty from its decreased signal to noise ratio. Because the methylene pattern is broader than the methine pattern, it contributes more to the outer sidebands. This means that if this sideband has lost some of its intensity into the noise level of the spectrum, then the ratio will err in favor of more methines. Looking at the figure, the fourth sideband gives solutions that lie toward a higher number of methines. A practical lesson from this analysis is that some care should be taken in the integration of the outer sidebands as they are somewhat wider. In cases where the signal to noise is poor at the outer sidebands, this method tends to give a minimum value for the methylene contribution.

Slices from the aromatic region clearly allow assignment of the nonprotonated and protonated carbon resonances. When the

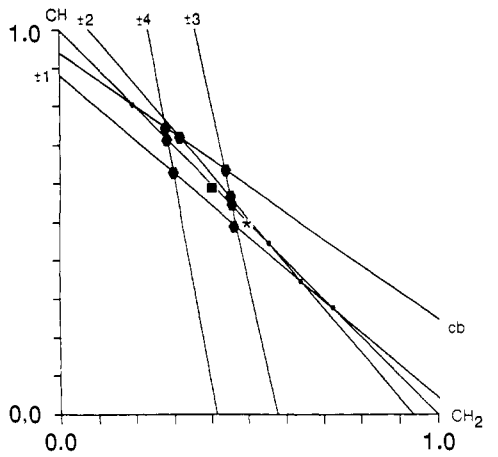

Figure 7. Plot of the equations generated by the sidebands in the MASSLF pattern for the CH plus CH_2 line in the polystyrene spectrum. The constraining equation is plotted diagonally between the points (1,0) and (0,1). Each intersection represents a possible solution. In the ideal case all lines would intersect in a single point on this plot. The actual ratio is indicated by a *. The average of the solutions obtained by the intersection of the sideband equations with the constraining equation is indicated by ■. The cluster of solutions about this average value are shown by ●, and further solutions are shown by •. Each line is labeled according to the sideband used to generate the line. Tables of the experimental integrated intensities used are available in the supplementary material.

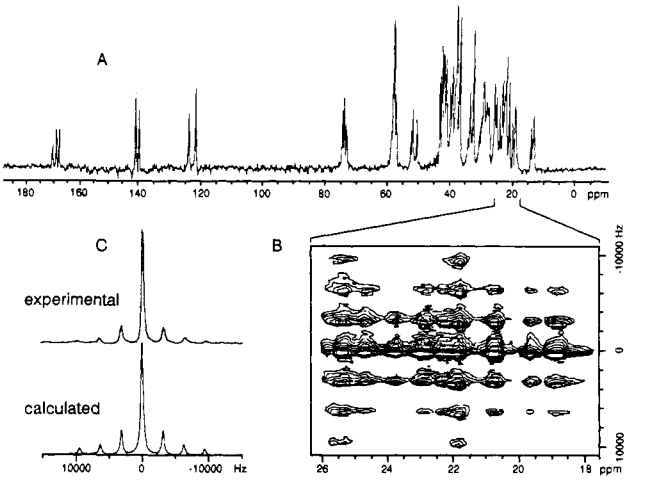

Figure 8. (A) ^{13}C CPMAS spectrum of cholesteryl acetate. Note that there are many more resonances than there are carbon centers in this molecule. (B) The contour plot of the MASSLF spectrum for this molecule in the 26- to 17-ppm region. (C) The experimental MASSLF pattern produced by summing all intensity in the 26- to 17-ppm region. The pattern calculated using the known ratios of the carbon types is shown for comparison. Again note that the ratios of integrated intensities are very close to one another. The discrepancies in peak heights are again due to the fact that the sidebands in the experimental spectrum are progressively wider for higher order sidebands, while the same line width is used for all sidebands in the calculated spectrum. The experimental integrated intensities are included in tables of supplementary material.

aromatic methine experimental integrated intensities are fit to nonprotonated and aromatic methine model sideband intensities, the expected result of all methines is obtained (see Figure A of the supplementary material).

Cholesteryl Acetate. The CPMAS spectrum for cholesteryl acetate in Figure 8 is quite complex and displays many more resonances than there are carbons in the molecule. In the carbonyl region there are three resonances indicative of at least three inequivalent molecules in the solid. This particular sample contains two different crystalline modifications.[53] Polymorph I has two inequivalent molecules in the unit cell and gives the pairs of lines

(53) Sawzik, P.; Craven, B. M. *Acta Crystallogr.* **1979**, *B35*, 895–901.

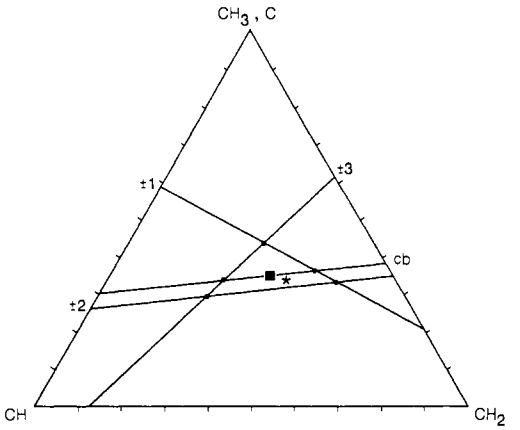

Figure 9. Triangular plot for the MASSLF sideband intensities from a pattern generated by summing all intensity in the 60- to 10-ppm portion of the cholesteryl acetate spectrum. Each intersection • represents a solution consistent with the constraint that the sum of the fractions of the three carbon types equals 1. The actual $CH:CH_2:C,CH_3$ ratio is indicated by an asterisk. The average of the experimental solutions is indicated by ■. The experimental integrated sideband intensities are contained in the tables of supplementary material.

of equal intensity in the spectrum. The other set of lines is due to polymorph II. It is interesting to note that the shift differences between the pairs of lines for the first polymorph are largest at positions closest to the magnetically anisotropic ester and alkene functionalities. In principle, these intermolecular chemical shifts contain some information as to the packing arrangement in these phases. Spectral overlap in the aliphatic region is fairly severe with up to five resonances being coincident in some regions. An expansion of the contour plot for the MASSLF spectrum 26–17 ppm region is shown in Figure 8, indicating the wealth of information contained in these data. Many assignments can be made on inspection, especially for the single resonances and for pairs of overlapping resonances. While most of the resonances can be assigned in this way, a comparison with the solution spectrum is necessary to distinguish some methyls from quaternary carbons.[54] From Roberts' solution assignment it is known that there are five methyls and three methylenes in this region. The MASSLF slice that results from summing all of the slices between 26 to 17 ppm as well as a computer simultation using this ratio of methyl to methylene carbons is shown in Figure 8. The agreement would be better if the simulated sidebands were given different widths, as they have in the experimental spectrum. The graphical sideband analysis method was applied (Figure B, supplementary material) as described before for polystyrene. A two-parameter fit to model sideband intensities gives a $\alpha_{CH_2}:\alpha_{CH}$ ratio of 5.8:2.2. As in the polystyrene case, the ratio errs toward a smaller value for the number of methylenes. When this MASSLF slice is fitted to methyl, methylene, and methine sideband intensities (Figure C, supplementary material), the fit clearly demonstrates that there are no methines in this region. The methyl to methylene ratio from the $\alpha_{CH_2}-\alpha_{CH_3}$ line agrees well with the two-parameter fit value.

An example of a three-parameter fit is shown in Figure 9 for the MASSLF spectrum from a 90° sum of the 60- to 10-ppm f_2 region. From Roberts' assignment, the $CH:CH_2:C + CH_3$ ratio in this region is known to be 6:11:8. The intensities used for the analysis are given in Table IX of the supplementary material. The positions of the average solution, corresponding to a 6.7:9.8:9.0 ratio, and the known ratio are noted on the triangular plot. Overlooking the centerband has little if any effect on the average value. The relative number of methines to methyls experimentally is the same as the true value, 3:4. The difference in the experimental and actual ratios is again mostly due to error in the number of methylenes, with the experimental value being smaller than the known value, consistent with earlier results.

(54) Reich, H. J.; Jautelat, M.; Messe, M. T.; Weigert, F. J.; Roberts, J. D. *J. Am. Chem. Soc.* **1969**, *91*, 7445–7454.

Conclusions

The asynchronous MASSLF method presented here promises to be a convenient technique for assigning complex ^{13}C CPMAS spectra in a variety of chemical systems. The experiment is unique in that all types of carbon centers are observed in a single experiment and it can be used to differentiate methines from methylenes. While the applications here were limited to ^{13}C spectroscopy, the method can be easily extended to any system of spin $^1/_2$ nuclei. The basic idea behind the method is that under the proper experimental conditions in rigid solids the MASSLF slices are principally determined by the number of protons attached to a ^{13}C center. For this to hold, the geometries of the various carbon centers, i.e., C–H distances and H–C–H angles, must not significantly vary from some characteristic set. Equivalently this can be stated by saying it is reasonable to assume that C–H distances in organic solids are 1.09 ± 0.01 Å, and that H–C–H angles are either 109 ± 5° for aliphatic methylenes, or 120 ± 5° for terminal alkenes.

The particular pulse sequence used here is relatively simple to implement given the appropriate hardware and software, and often permits assignment of spectra on inspection. The advantage of this sequence over other MASSLF methods is that synchronization with the MAS rotation is not required, a large f_1 bandwidth is easy to achieve, and the effect of quadrature detection in t_1 is easily mimicked by using time proportional phase incrementation. For assignment of spectral lines in pure compounds, the graphical method outlined here typically provides sufficient accuracy to determine the methylene:methine:quaternary plus methyl carbon ratios to within ±1 carbon. The principal limitations of the method in this regard are most likely due to the usual difficulties encountered in accurately integrating spectral peaks, and the intensity distortions inherent in CPMAS spectroscopy itself, rather than any of the underlying assumptions in the method presented here.

Acknowledgment is made to the donors of the Petroleum Research Fund administered by the ACS for partial support of this work. Primary support for this project was provided by the Department of Energy under the Fossil Energy Program, Grants DE-FG22-83PC60791 and DE-FG22-85PC80508. The gift of software by Dr. Andrew Byrd is gratefully acknowledged. Helpful discussions with Dr. Alan Berger and with Dr. R. G. Griffin on the computer calculation of spinning sideband intensities are acknowledged, and the authors thank Dr. Joel Garbow for suggesting polystyrene as a useful model polymer. Computer programming by Mr. J. S. Plank and Dr. R. A. Merrill, and the assistance of Mr. J. C. Duchamp in the computer sideband calculations, is gratefully acknowledged.

Supplementary Material Available: Tables listing calculated MASSLF sideband intensities for CH and CH_2 groups of varying geometry with and without chemical shift anisotropy and tables of experimental MASSLF sideband intensities for polystrene and cholesteryl acetate and plots of the aromatic CH resonance in polystyrene and $\pm n$ sideband and centerband equations for Figure 9C (12 pages). Ordering information is given on any current masthead page.